The Cryosphere Discuss., 8, 1151–1189, 2014
www.the-cryosphere-discuss.net/8/1151/2014/
doi:10.5194/tcd-8-1151-2014

The Cryosphere Discussions
Open Access

Simulating the Greenland ice sheet under present-day and palaeo constraints including a new discharge parameterization

R. Calov[1], A. Robinson[1,2,3], M. Perrette[1], and A. Ganopolski[1]

[1]Potsdam Institute for Climate Impact Research, Potsdam, Germany
[2]Universidad Complutense Madrid, 28040 Madrid, Spain
[3]Instituto de Geociencias, UCM-CSIC, 28040 Madrid, Spain

Received: 22 January 2014 – Accepted: 4 February 2014 – Published: 17 February 2014

Correspondence to: R. Calov (calov@pik-potsdam.de)

Published by Copernicus Publications on behalf of the European Geosciences Union.

Abstract

In this paper, we propose a new sub-grid scale parameterization for the ice discharge into the ocean through outlet glaciers and inspect the role of different observational and palaeo constraints for the choice of an optimal set of model parameters. This parameterization was introduced into the polythermal ice-sheet model SICOPOLIS, which is coupled to the regional climate model of intermediate complexity REMBO. Using the coupled model, we performed large ensemble simulations over the last two glacial cycles. We exploit two major parameters: a melt parameter in the surface melt scheme of REMBO and an ice discharge parameter in our parameterization of ice discharge. Our constraints are the present-day Greenland ice sheet surface elevation, surface mass balance partition (ratio between ice discharge and total precipitation) and the Eemian interglacial elevation drop relative to present-day in the vicinity of the NEEM ice core. We show that the ice discharge parameterization enables us to simulate both the correct ice-sheet shape and mass balance partition at the same time without explicitly resolving the Greenland outlet glaciers. For model verification, we compare simulated total and sectoral ice discharge with those from other findings, including observations. For the model versions, which are inside the range of observational and palaeo constraints, our simulated Greenland ice sheet contribution to Eemian sea level rise relative to present-day amounts to 1.4 m on average (in the range of 0.6 and 2.5 m).

1 Introduction

Modelling the response of the Greenland Ice Sheet (GIS) to anthropogenic warming has already been undertaken for more than two decades (Huybrechts et al., 1991; van de Wal and Oerlemans, 1997; Huybrechts and de Wolde, 1999; Greve, 2000) and attracted considerable attention in recent years (Vizcaíno et al., 2010; Goelzer et al., 2011; Graversen et al., 2011; Applegate et al., 2012; Lipscomb et al., 2013; Stone et al., 2013), including higher-order and full-Stokes modelling approaches (Price et al., 2011;

TCD
8, 1151–1189, 2014

Seddik et al., 2012; Goelzer et al., 2013). The recent SeaRISE ice sheet modelling project (Nowicki et al., 2013) highlighted the importance of treatment of processes at the ice-ocean interface for the response of models of the Greenland ice sheet to future climate change.

Observational data indicate that during the past decade mass loss by the GIS, both through surface melt and enhanced ice discharge, has contributed appreciably to global sea level rise (Shepherd et al., 2012). The latest projections suggest that the GIS will contribute notably to sea level rise during the next century (Hanna et al., 2013). In the longer-term perspective, the GIS can become even more important, because even if the global temperature is stabilised at the level of 2 °C above preindustrial, the GIS would still continue to melt and, in the long-term perspective, can lose a significant fraction of its mass even for moderate warming (Ridley et al., 2005; Robinson et al., 2012).

Models of the GIS contain a number of parameters, which can be used for tuning the model using observational constraints. Present-day extent and surface elevation of the GIS are accurately known and it is natural to use them as such constraints (e.g. Stone et al., 2010; Greve et al., 2011; Lipscomb et al., 2013). At the same time, it is known that coarse-resolution ice-sheet models have problems in simulating the correct margins of the GIS and they systematically overestimate its volume. One reason is that under present-day conditions, most ice discharge into the ocean occurs through relatively narrow outlet glaciers. As a result, although ice discharge into the ocean currently accounts for more than half of surface accumulation, over most of Greenland the ice sheet margin is located several tens of kilometres away from the ocean. Since current ice-sheet models do not resolve outlet glaciers and their interaction with the ocean in the fjords, the modelled GIS needs too much contact with the ocean to produce realistic discharge. This leads to systematic overestimation of the ice area and volume and makes observational "geometrical" constraints difficult to apply.

However, the observed shape of the GIS is not the only characteristic that can serve as a constraint for the GIS models. Recently, Robinson et al. (2011) introduced the

TCD
8, 1151–1189, 2014

mass balance partition (defined as the ratio between ice discharge into the ocean and total precipitation over the GIS, MBP) as another constraint on the GIS. The MBP is an important characteristic for short-term as well as for long-term (future) behaviour of the GIS, because it determines the GIS mass balance sensitivity to climate change. In particular, the present-day MBP is related to the long-term stability properties of the GIS (Robinson et al., 2012), i.e. for low MBP values (large surface melt) the modelled GIS is more susceptible to warming than for high ones. For the long-term stability of the GIS, the MBP is a more important characteristic than the present-day shape of the GIS. However for short-term (centennial time scale) future global warming simulations, such an ice sheet would be an unfavourable initial condition, because during a considerable portion of time of such a future simulation the modelled ice would melt in areas, where in reality no ice exists (Goelzer et al., 2013). Since standard coarse-resolution GIS ice sheet models cannot simulate a realistic present-day extent/surface orography of the GIS and at the same time have the correct mass balance partition, we developed a novel approach, which allows us to circumvent this problem, without resolving individual ice streams and outlet glaciers – and without an increase in computational cost. This approach is in the spirit of our previous modelling work (Robinson et al., 2010, 2011, 2012) and is based on a rather simple semi-empirical parameterization of ice discharge through the outlet glaciers. We propose the usage of this approach until a more complete representation of fast processes is available. Considering the above concerns, this approach is feasible for short-term as well as for long-term simulations.

In addition to the present-day constraints on the ice-sheet shape and the MBP, we use the Eemian as a palaeo constraint. Eemian conditions have already been recognized earlier as an important palaeo constraint for GIS model parameters (Tarasov and Peltier, 2003) and have been applied more recently in several studies (Robinson et al., 2011; Born and Nisancioglu, 2012; Stone et al., 2013). While the Greenland Summit position might be located too far in the interior of the GIS to serve as a strong palaeo constraint, the position of the new NEEM ice core appears more promising, because it is located rather near the ice margin, a location which is very sensitive to the

TCD
8, 1151–1189, 2014

climate changes during Eemian (Born and Nisancioglu, 2012). In the present paper, we make use of the recently published estimate of the Eemian elevation drop at a position of about 200 km upstream of NEEM (NEEM community members, 2013), where the borehole ice sampled today was deposited during Eemian.

The paper is summarized as follows. First, we give a short description of the ice-sheet model SICOPOLIS and the regional energy-moisture balance model REMBO (Sect. 2). Our new discharge parameterization is comprehensively explained in Sect. 3. Different metrics of model performance are introduced and discussed in Sect. 4. In Sect. 5, we describe our constraints and simulations and compare our findings with those of others, as well as with observations. We close with a discussion and finally our conclusions.

2 Model description

For this study, we used the three-dimensional polythermal ice-sheet model SICOPOLIS (version 2.9) coupled to the regional energy-moisture balance model (REMBO). SICOPOLIS treats the evolution of ice thickness, ice temperature and water content (Greve, 1997) based on the shallow ice approximation. The dependence of the ice velocities on the ice temperature and water is introduced via the rate factor. SICOPOLIS enables a free and easy choice of several parameters including resolution. In our paper, Greenland is mapped onto a stereographic plane with 76 × 141 grid points (20 km grid spacing) using the topographic dataset by Bamber et al. (2001). The vertical is resolved by 90 layers with decreasing layers thickness towards the bed of the ice sheet. A 10-layer thermal rock bed is coupled to the overlying ice sheet via heat fluxes. The geothermal heat flux is prescribed at the lower border of the thermal bedrock. The bedrock adjusts to the load caused by the ice sheet's weight using a local lithosphere relaxing asthenosphere model with a time delay of 3000 yr.

The regional energy-moisture balance model REMBO is a climate model of intermediate complexity and it is described in detail in Robinson et al. (2010). REMBO uses

TCD
8, 1151–1189, 2014

diffusion-type equations for surface air temperature and atmospheric water content. For temperature, the well-known Budyko–Sellers energy balance approach is implemented. Planetary albedo is related to surface albedo via a linear parameterization based on empirical data. The lateral boundary conditions for temperature and relative humidity are taken from climatology (Uppala et al., 2005) for the years 1958–2001, which in this paper is referred to as "present-day". REMBO includes a 1-layer snowpack model with a simple parameterization of refreezing. Surface albedo depends on snow thickness and the melt rate. Surface melt is computed using a simple parameterization of van den Berg et al. (2008) and depends on both temperature and insolation. The formula for surface melt contains a free parameter c_m (melt parameter), which is one of the major parameters determining the sensitivity of the ice sheet to climate change (Robinson et al., 2011). It reads

$$m = \frac{\Delta t}{\rho_w L_m}[\tau_s(1-\alpha_s)S + c_m + \lambda T], \quad (1)$$

which relates the potential surface melt m with the free melt parameter c_m. The remaining variables Δt, ρ_w, L_m, τ_s, α_s, S, λ and T, are the day length, the density of water, the latent heat of ice melting, the total transmissivity, the surface albedo, the insolation at the top of the atmosphere, the long wave radiation coefficient and the surface temperature, respectively. Please, refer to (Robinson et al., 2011) for more details.

The coupling between the models is bi-directional, i.e., SICOPOLIS provides the climate model with information about surface elevation and spatial extent of the ice sheet. In turn, REMBO provides SICOPOLIS with surface mass balance and mean annual surface temperature.

3 Ice discharge parameterization

Ice discharge is considered as a sub-grid process and is parameterized in a simple heuristic-statistical approach. The mass loss d in the grid cell (i, j) due to the ice

TCD
8, 1151–1189, 2014

discharge into the ocean is parameterized as

$$d = c\frac{h^p}{l^q}, \quad \text{defined over } \Delta R, \tag{2}$$

where l and h are the distance from the actual grid cell (i, j) to the nearest ocean grid cell and the ice thickness, respectively. They are the two major variables, which control the ice discharge. The parameterization applies to any grid point located within a distance ΔR from the nearest ice-free land surface points (note ΔR only determines whether the parameterization applies or not, but plays no role for the actual value of the discharge; see Fig. 1 for an illustration).

The parameter c varies strongly for different values of the powers p and q to maintain constant discharge. For convenience, we normalize c as

$$c = c_0 c_\mathrm{d}, \tag{3}$$

i.e., for any fixed value of p and q we selected c_0 such that c_d has a value of about one. In practice, after selecting p and q we chose c_0 so that the parameterization applied to observed Greenland elevation matched observed total discharge, for which we used $350\,\mathrm{Gt\,yr^{-1}}$. The latter value is just about the average of the totals of ice discharge as found by Reeh (1994) and (Rignot et al., 2008). Although the discharge for the modelled present-day GIS will not be precisely $350\,\mathrm{Gt\,yr^{-1}}$, such an approach guarantees that all valid values of the parameter c_d maintain the order of magnitude of about one for any power p and q.

We thus have three free ice-discharge parameters c_d, p and q in our parameterization (Eqs. 2 and 3). Based on an ensemble of model simulations, we chose $p = 1$ and $q = 3$ for the powers, and the range of valid c_d was selected using the observational constrains as it is described below (Sect. 5.1). For the above powers, we fix the dependent parameter as $c_0 = 2.61 \times 10^4\,\mathrm{m^3\,s^{-1}}$. Both the discharge parameter c_d and the melt parameter c_m determine the major characteristics of the GIS. Therefore, a set of valid model versions is determined by paired values of c_d and c_m.

TCD
8, 1151–1189, 2014

Additionally, we assume that ice discharge only occurs if the inland-ice surface is descending toward the coast. This is enforced by setting a maximum value of $\alpha_0 = 60^\circ$ to the angle between the gradients of surface elevation ∇z_s and distance field ∇l (see Fig. 2 for the characteristics of the field l). Using the definition of the scalar product for the angle between above two gradients this reads

$$\frac{\nabla z_s \cdot \nabla l}{|\nabla z_s||\nabla l|} \geq \cos(\alpha_0), \quad \text{evaluated at } (i, j). \tag{4}$$

This prevents our parameterization from simulating ice discharge into the ocean from an ice margin, which is oriented towards the interior of the Greenland island, which could happen when the GIS is retreating under warm climates and only a few small ice sheets remain, see the small land bridge between the two ice caps in Fig. 3b for example.

The discharge parameterization is applied only to the ice covered grid cells which are located not more than ΔR (here $\Delta R = 120\,\text{km}$) from the ice margin (see Fig. 1). The resulting belt encloses the regions of ice with rather high velocities as found by satellite measurements (Joughin et al., 2010; Rignot and Mouginot, 2012). The idea here is to largely capture two aspects of fast ice flow with this parameterization: the fast outlet glaciers themselves, as well as the rather fast flowing ice in the catchment regions upstream of the outlet glaciers. The ice thickness h describes the amount of ice that can be brought to the outlet glaciers. And the power of the inverse distance to the coast $(1/l)^q$ can be regarded as a statistical measure of the outlet glacier density: if the ice margin is far away from the coast, it is very unlikely that any outlet glacier has contact with the ocean and there is only minor calving flux into the ocean, while one would expect a large calving flux for small distances to the coast.

Although the parameterization by Eq. (2) mimics non-resolved lateral ice discharge, the term d has the dimension $\text{m}\,\text{s}^{-1}$. The term is directly included in the evolution equation of ice thickness evolution as

$$\frac{\partial h}{\partial t} = -\nabla \cdot \boldsymbol{q} + b + d, \tag{5}$$

TCD
8, 1151–1189, 2014

where $\boldsymbol{q}$ and b are the lateral mass flux and the surface mass balance, respectively. Unlike the surface mass balance, the ice discharge d in our model depends only on the ice-sheet geometry.

As seen in Fig. 2, the minimal distance to the coast l can reach up to about 400 km in the centre of Greenland. In our parameterization, the inverse dependence of the ice discharge on the minimal distance to the coast – here even to the third power – is a condition for high ice discharge over regions with small minimal distance (dark brown colour) and low discharge further inland (lighter brown colours). For a minimal distance of around 400 km the parameterized ice discharge would nearly vanish. In our discharge parameterization, this is relevant for an ice sheet under warmer climates, which can be smaller than the present-day GIS. Recall that our parameterization only applies for $\Delta R < 120$ km around the ice margins. One can see that the observed present-day Greenland near-margin ice area largely covers regions with small minimal distances. These are the regions where a high present-day ice discharge due to many outlet glaciers is observed (e.g. Moon et al., 2012), e.g. over the north-western region of the GIS. For regions with fewer marine outlet glaciers, e.g. in the south-west, the observed ice margin resides rather in regions with larger minimal distances.

As stated above, our discharge parameterization is not intended to resolve every small individual outlet glacier; it is rather designed to capture their draining effect on spatial and temporal average in a sub-grid scale statistical approach. In general, our simulated present-day ice discharge (Fig. 3a) is high over regions with many observed outlet glaciers and low over regions with fewer observed outlet glaciers, see Fig. 3 in Moon and Joughin (2008) for comparison. However, in the south-western part of Greenland we overestimate the ice discharge, in part due to too high simulated accumulation over that region (compare Sect. 5.3).

Our discharge parameterization is capable of simulating ice discharge even without explicit contact of the simulated ice sheet with the ocean, see the narrow brown coastal land stripes in Fig. 3. This is possible, because our discharge parameterization by its construction does not need to resolve explicitly the fine structure of outlet glaciers

TCD
8, 1151–1189, 2014

and fjords. In particular, this means if our parameterized ice discharge is strong – i.e., the valid c_d is sufficiently large –, then there is practically no explicit SICOPOLIS ice discharge, since GIS is not in direct contact with the ocean in this case. It can be seen that for large distances of the ice margin to the coast there is less ice discharge than for small distances, as intended with our parameterization.

4 Measures of geometrical characteristics of an ice sheet

There are numerous possibilities to define a measure of the performance of a model based on the comparison of simulated geometrical characteristics of an ice sheet with observational data. The simplest is to use the error in simulated total ice area and ice volume, which we define as

$$\mathrm{err}(A) = \frac{|A_{\mathrm{mod}} - A_{\mathrm{obs}}|}{A_{\mathrm{obs}}} \cdot 100, \quad \mathrm{err}(V) = \frac{|V_{\mathrm{mod}} - V_{\mathrm{obs}}|}{V_{\mathrm{obs}}} \cdot 100, \tag{6}$$

where A_{obs}, A_{mod}, V_{obs} and V_{mod} are the observed ice area, the modelled ice area, the observed ice volume and the modelled ice volume, respectively. These errors in principle can approach zero, but this does not guarantee accurate simulation of the ice-sheet geometry, since regional errors can compensate each other. Therefore, we choose a stronger constraint based on the error in ice thickness expressed relatively to the total ice thickness. This reads

$$\mathrm{err}(H) = \frac{\sum_{ij} |H_{ij}^{\mathrm{mod}} - H_{ij}^{\mathrm{obs}}|}{\sum_{ij} H_{ij}^{\mathrm{obs}}} \cdot 100, \tag{7}$$

where H_{ij}^{obs} and H_{ij}^{mod} are, respectively, the observed and measured ice thickness at the horizontal grid position (i, j). The indices i, j run over the entire domain of the computational area and assume that the ice thickness is zero outside the ice covered area.

TCD
8, 1151–1189, 2014

This error only approaches zero when the ice-sheet thickness is correctly simulated in each grid cell.

Figure 4 compares the three error measures for the ice-sheet shape in the phase space of the melt, c_m, and discharge, c_d, parameters. At first sight, the error fields in the three panels look similar. The smallest errors appear approximately along the descending diagonal, which is characterised by decreasing values of c_m and increasing values of c_d. One can also see that the parameter combinations with small errors are not limited to our sampled space: these regions expand in the direction of the descending diagonal. This underlines the need for more constraints (Sect. 5.1).

Figure 4 illustrates that our discharge parameterization allows us to reduce the errors in total area and volume practically to zero. However, we found no parameter combination for which the error in ice thickness was much lower then 20 %. Still, these are considerable improvements compared to standard version of the model without ice discharge parameterization constrained only by the mass balance partition (Robinson et al., 2011), which overestimates total ice volume and area by ca. 20 % and has a relative thickness error of ca. 30 %. When the mass balance partition is ignored, one can improve model performance by increasing surface melt. By choosing $c_m = -40\,\mathrm{W\,m^{-2}}$, one can make all three errors comparable with those of the best model version with ice discharge parameterization. However, such a high melt factor practically eliminate ice discharge into the ocean and, as shown below, drastically affects the GIS stability. In fact, it causes the GIS to be unstable even under near present-day climate conditions.

5 Results

5.1 Model setup and constraints

Following Robinson et al. (2011), we run the coupled REMBO-SICOPOLIS model through two glacial cycles starting at 250 kyr BP. These simulations serve a dual purpose: to perform a model spin-up necessary to simulate the present-day state of the

TCD
8, 1151–1189, 2014

GIS and to apply palaeoclimate constraints (see below) to additionally reduce the range of model parameters. To drive the model through two glacial cycles, we apply variations in insolation due to changes in orbital parameters, CO_2 concentration and regional temperature anomaly obtained from the CLIMBER-2 model (Petoukhov et al., 2000; Calov et al., 2005). We took these anomalies from the standard simulation as in Ganopolski and Calov (2011). To generate an ensemble of model realisations, we vary two parameters: the discharge parameter c_d (Sect. 3) and the melt parameter c_m. The discharge parameter c_d is varied in steps of 0.2 and the melt parameter c_m in steps of $5\,W\,m^{-2}$. The geothermal heat flux is set to $50\,mW\,m^{-2}$ and the sliding coefficient to $15\,m\,(yr\,Pa)^{-2}$. All other parameters are the same as in Robinson et al. (2010).

As constraints on the ensemble, we use the relative error in present-day ice thickness (see Sect. 4), the present-day surface mass balance partition and the Eemian drop in surface elevation relative to present-day upstream of the ice borehole position NEEM. Figure 5a–c illustrates all constraints used in this paper.

We accept a value of 20 % for the error in ice thickness. This choice is not totally arbitrary, because a closer inspection of the error field shows a minimum error in ice thickness of 18.2 %, i.e., there is indeed a plateau defined by ice thickness error values ≤ 20 %, as illustrated in Fig. 5a by the medium green shading. Within the parameter space, the error in ice thickness varies much more strongly for values higher than 20 %. This supports the latter value as a reasonable constraint for the determination of valid parameters.

As mentioned in the introduction, the mass balance partition is the amount of ice discharge compared to precipitation. In our work, we always refer to MBP as a characteristic of the ice sheet defined in its present-day state. Its practical definition is the total ice discharge divided by the total precipitation for the simulated present-day ice sheet. In Robinson et al. (2011), the MBP was diagnosed by REMBO from simulations with prescribed observed present-day ice-sheet topography. This was done because of systematic (and regionally significant) deviations of the simulated present-day GIS from observational data. With the ice discharge parameterization, we can now safely

TCD
8, 1151–1189, 2014

operate with the simulated present day ice-sheet topography for determining MBP, because of the better match between simulated and observed topography. This means that our new MBP values simulated with ice discharge parameterization slightly differ from our former approach ($c_d = 0$), and the valid MBP range (Fig. 5b) corresponds to somewhat lower values of c_m compared to those by Robinson et al. (2011). However, the MBP has large inherent uncertainty, which we derived from regional climate models, following Robinson et al. (2011) and yielding a range of 45 % to 65 %.

From measurement of air content in the NEEM borehole samples, the NEEM community members (2013) found that the surface elevation was 130 ± 300 m lower during Eemian than at present-day, which we exploit as our third constraint. Following these findings, we assume the maximal surface elevation drop at this location during Eemian (130 to 115 kyr BP) did not exceed 430 m (compared to present-day). Accounting for the trajectory tracing results by NEEM community members (2013), we used the deposition position of NEEM, a location about 200 km upstream from NEEM at (45° W, 76° N) (see Fig. 7d), denoted NEEMup hereafter. This upstream position is the location where the sampled NEEM ice was deposited by snowfall during Eemian, carrying the air composition at that upstream position, which therefore is the location at which the Eemian change in surface elevation happened.

Figure 5a–c illustrates that none of the constraints is redundant, because the regions of valid simulations for all three constraints intersect each other and there is plenty of space without a common crossover for every constraint. In particular, the error in thickness excludes low values of the ice discharge parameter, while the mass balance partition constrains the range of the melt parameter, the upper bound of which is then further constrained by the NEEMup elevation data. While the valid region of all three constraints cover an about equally large part of the parameter space (Fig. 5a–c), only a relatively small subset of model parameters (Fig. 5d) is consistent with all of these constraints simultaneously.

Figure 6 shows all possible ice margins which are consistent with the different constraints. It can be seen that the MBP constraint alone (Fig. 6a) gives a rather broad

TCD
8, 1151–1189, 2014

band of valid ice margins, while the NEEMup constraint (Fig. 6b) alone results in an ice margin range, which is quite comparable with that of the err(H) constraint (Fig. 6c). Finally, all three constraints together give a pronounced reduction of spread of ice margins (Fig. 6d) compared to the single-constraint cases. Simulated ice margins in the south, mid-west and northeast of Greenland compare well with observations. However, there are regions with rather strong mismatch in the southwest and in the north. Parts of this mismatch can be attributed to our model biases in precipitation. For example, REMBO simulates too much snow accumulation in the northeast and southwest of Greenland compared to the compilation by Bales et al. (2009).

Figure 5d depicts the simulated difference in GIS volume between Eemian and present-day expressed in units of global sea level. Compared to the other figure panels, we show here results from simulations with the refined melt parameter spacing of $1\,\mathrm{W\,m^{-2}}$. We enhanced the resolution of the melt parameter sampling, because the region of valid simulations appears rather elongated in the parameter space. The estimated Eemian sea level contribution increases with increasing values of c_m. This is understandable, because surface melting increases with larger melt parameter values. Nevertheless, there is also an increase of the GIS contribution to the Eemian sea-level highstand for increasing discharge parameter values. Obviously, there is an interplay between ice discharge and surface melt, because the ice discharge removes ice from the ice sheet and brings the ice surface into lower regions of the atmosphere, where stronger surface melt can occur. Averaged over the parameter space of valid simulations, we have a contribution of the GIS to Eemian sea level rise (above present-day value) of 1.4 m. The minimum contribution of the GIS sea level rise among all valid simulations is 0.6 m and the corresponding maximum is 2.5 m.

5.2 Eemian vs. present-day and GIS stability

Figure 7 shows the simulated present-day and Eemian ice distributions from model versions with high, medium and low sea-level rise contributions (2.5, 1.5 and 0.6 m) of the Eemian compared to present-day. While all fields look rather similar for the present-day,

TCD
8, 1151–1189, 2014

there is a considerable difference between the corresponding Eemian fields. However, the present-day surface elevations for the different valid parameters sets still show slight differences. Naturally, these differences appear mainly near the ice margin, while the interior of the ice sheet remains almost unchanged for any valid parameter set. As is often the case in such optimization problems, there is a trade-off concerning agreement with observations in certain regions (see Fig. 9a for the observed surface elevation). While the simulation with $c_d = 0.8$, $c_m = -53\,W\,m^{-2}$ (Fig. 7a) better resembles the ice-free southwestern region, the northern region around Petermann Gletscher matches the observation less well. This situation is opposite for the simulation with $c_d = 1.2$, $c_m = -66\,W\,m^{-2}$ (Fig. 7c).

For all valid parameter sets, our simulated reduction in Eemian ice volume is accompanied by a strong retreat of ice in Greenland in particular in its northern part, see Fig. 7d–f, which spans simulated lowest and highest Eemian to present-day GIS contribution to sea level drop. For model versions with high sensitivity to climate forcing, the GIS splits into two parts: a small ice cap in southern Greenland and a larger ice sheet in central Greenland (Fig. 7d). For the intermediate and low sensitivity model versions, the GIS remains in one piece (Fig. 7e and f). In all valid model versions, there is a strong retreat of ice, mainly in western and northern Greenland. Our estimates showing a strong retreat of the GIS during Eemian rather correspond to the simulations by Otto-Bliesner et al. (2006), while the medium to modest retreat of the Eemian GIS was found in simulations by Helsen et al. (2013) and Quiquet et al. (2013).

Interestingly, the NEEM location almost becomes ice free at 121 kyr BP in our most sensitive model version, see Fig. 7d. Nonetheless, an ice free NEEM position during Eemian would not contradict the existence of Eemian ice and most probably pre-Eemian ice in the NEEM ice core at present-day, as reported by NEEM community members (2013), since the Eemian ice was accumulated farther upstream of NEEM. Similar argumentation would hold for Camp Century as well.

Figure 8 shows time series of ice volume and the NEEMup surface elevation for simulations over the last two glacial cycles from previous work with the same model

TCD
8, 1151–1189, 2014

(Robinson et al., 2011) and our present approach, which includes the sub-grid scale discharge parameterization. At all times, the valid model versions with the discharge parameterization simulate less ice volume than that without the discharge parameterization (Fig. 8a). This has two reasons: (i) previously, the model was not tuned for agreement with present-day surface elevation (ice volume). The present-day surface mass balance partition was (and is here) regarded as the more adequate characteristic to capture the sensitivity of the GIS to long-term climate change. (ii) In our present approach, the inclusion of the discharge parameterization enables our rather coarse resolution model to mimic the calving of the small-scale outlet glaciers (i.e. removal in ice into the ocean by ice discharge) without an overestimation of contact regions of the ice sheet with the ocean, which leads to a smaller ice sheet.

Additionally, two extreme and unrealistic simulations, depicted by the red lines, were set up in order to demonstrate, what happens when a shape-only tuning applies in a coarse-resolution model, which disregards fast sub-grid processes of small outlet glaciers. Technically, we restrict the parameter space by setting $c_d = 0$ (discharge parameterization off) and minimize the error measure err(H) and, alternatively, the weaker error measure err(V) to get the right present-day shape. The former belongs to the parameter setting $c_d = 0$, $c_m = -42\,\mathrm{W\,m^{-2}}$ and the latter to $c_d = 0$, $c_m = -40\,\mathrm{W\,m^{-2}}$. Please, note that these melt parameter values are outside the valid range of MBP as determined by Robinson et al. (2011) using observed present-day topography as well as outside the valid c_m values in MBP space of this work (Fig. 5b) using simulated present-day topography to determine MBP. Because we consider the present-day ice-sheet shape as the only constraint (for demonstration), the model without the discharge parameterization ($c_d = 0$) appears to perform well in the c_m space, but the melt parameter c_m becomes rather high for all minimized shape errors (Fig. 4). As one can see in Fig. 8a, around present-day the red line belonging to minimal err(H) is very close to the upper value of the range of the simulations with sub-grid discharge parameterization (blue shading), while the other red line (minimal err(V)) even merges with that valid range. Simulated present-day elevations at NEEMup lie rather close to each other in

TCD
8, 1151–1189, 2014

different model versions. However, during the Eemian interglacial, the runs from the shape-only constraints show strong downward excursions for ice volume as well as for the NEEMup elevation (Fig. 8b). Whether such a small Eemian ice volume is still realistic might be disputable. Nevertheless, the Eemian reduction in NEEMup elevation is by far larger than that estimated from the ice core (NEEM community members, 2013). The Eemian NEEMup position was even ice free in the shape-only simulation with minimized err(V), which certainly contradicts observational data.

Moreover, the strong drop in Eemian sea level and NEEMup elevation hints at very different stability properties of the model version with shape-only tuning in a coarse resolution model compared to all our valid model versions, which are still on coarse resolution, but contain our sub-grid scale discharge parameterization. Namely, the models with shape-only tuning are much more unstable than all the model versions that are constrained using the MBP and palaeo data. Most important, both of our sets of model versions are more stable than those models with shape-only tuning of melt parameter: the valid model versions of our former approach without discharge parameterization (Robinson et al., 2011, 2012) as well as our present ones with discharge parameterization. To achieve more meaningful information about the stability of the system, we performed an analysis based on many steady state runs over 300 kyr as in Calov and Ganopolski (2005), but in temperature space instead of insolation space. From those simulations, we obtain thresholds of decay of the GIS between 1.25 °C and 2.5 °C for the model versions with the discharge parameterization, depending on the position in parameter space (see also Table 1). The threshold estimated with the shape-only setting with err(V) minimisation ($c_d = 0$, $c_m = -40\,\mathrm{W\,m^{-2}}$) is much lower – only 0.25 °C. The higher values for GIS decay between 1.25 °C and 2.5 °C from our new REMBO-SICOPOLIS version with discharge parameterization are in the range of those that we found previously without using the discharge parameterization (Robinson et al., 2012). This similarity clearly is an implication of the use of the MBP as one common constraint in both approaches. In this work, the shape and palaeo constraints are important as well, because they cover different regions in parameters space as discussed

TCD
8, 1151–1189, 2014

in Sect. 5.1. It should be noted that a complete uncertainly analysis with our new model version is planned in the future, which will likely widen the range of our estimates.

In summary, whether we optimize the melt parameter in the coarse resolution model for err(H) or err(V), the resulting simulations all violate the MBP criterion. This leads to a strong drop of the NEEM elevation far below the one reconstructed from palaeo data, and the Greenland ice sheet becomes too instable. This is why (Robinson et al., 2011) and (Robinson et al., 2012) used the MBP criterion together with a palaeo constraint for calibration of their coarse resolution model, ensuring the correct long-term stability properties reported in this work. In our improved model with sub-grid scale discharge parameterization, we found a stability behaviour similar to that by Robinson et al. (2012) when using the MBP and NEEMup constraints, but now – still in the coarse resolution ice-sheet model – we can additionally fulfil a strong present-day shape constraint (err(H) $< 20\,\%$). We expect that all our constraints will play a similar role in a model of the Greenland glacial system which explicitly describes small-scale fast processes. Development of such a model is in our future plans.

One major advantage of our simple parameterization is that it applies easily for climates far away from present-day – a fully explicit modelling of present-day outlet glaciers could break down for the Eemian, because many present-day outlet glaciers just vanish in the Eemian. Figure 3a and b compares simulated ice discharge during present-day and Eemian. The present-day ice-discharge field was discussed already in Sect. 3. Here, we demonstrate that the regions of fast flow can reduce drastically for the Eemian time period compared to the present-day state. For the Eemian, there is practically no ice discharge over regions far away from the coast. In particular, the land bridge between the large ice sheet in the north and the smaller ice cap in the south of Greenland shows vanishing ice discharge. In general, our model results suggest that during the Eemian from the eastern coast of Greenland, more ice calves into the ocean than from its western coast. In particular, the Kangerlussuaq Gletscher region delivers ice into the ocean during Eemian in all our valid model versions.

TCD
8, 1151–1189, 2014

5.3 Comparison with present-day observations and findings by others

A direct comparison of our simulated Greenland surface elevation with the observed elevation by Bamber et al. (2001) and the former approach of Robinson et al. (2010) is shown in Fig. 9. Overall, we improved agreement with observations significantly. In particular, in the simulation with the discharge parameterization several regions are now ice-free, which look very similar to reality. The remaining deficiencies are partly due to the simple discharge parameterization and the limitations in the REMBO climatology, e.g., biases in representation of precipitation as discussed earlier. In this context, we would like to stress, that our model is a fully interactive one, where no observational data over Greenland are prescribed. This ensures that REMBO is applicable to climates far away from the present state, what is vital because the Eemian climate can deliver additional constraints for the model.

Figure 10 compares our simulated present-day sectoral and total ice discharge with findings by others. The sectors (see inset in the upper right of Fig. 10) correspond with those of Reeh (1994) and sub-divide the GIS into a northern (sector N), north-western (sector NW), north-eastern (sector NE), south-western (sector SW), and south-eastern (sector SE) part. This subdivision is also adequate to the degree of complexity (Claussen et al., 2002) of our model in its current stage of development (a refinement of the sectors is planned for our later work). Except for Ettema et al. (2009), all data shown are indicated as ice discharge in the respective papers. Ettema et al. (2009) presented surface mass balance simulated by the regional climate model RACMO2/GR. We used their simulated surface mass balance as ice discharge from the corresponding GIS regions assuming the GIS was in quasi-equilibrium over their time span 1958–2007, which is of course a rather crude assumption (see discussion below).

Over the sectors N and SW, our simulated range of ice discharge compares well with the findings of the others. While our simulated ice discharge range is somewhat low over sector NW, it is certainly too high over sector NE. The latter can be explained by

TCD
8, 1151–1189, 2014

the overestimation of our simulated present-day accumulation over sector NE by some 10 $Gt yr^{-1}$ compared to the compilation by Bales et al. (2009). In sector SE, our results are consistent with Reeh (1994) and Rignot et al. (2008) but are significantly lower than those by Ettema et al. (2009). We note that RACMO2/GR simulates much higher precipitation over that sector compared to REMBO and to observational estimates (Bales et al., 2009; Ohmura and Reeh, 1991). However, Ettema et al. (2009) argue that the higher precipitation results from a better representation of topography in their model compared to earlier approaches, i.e., the better spatial resolution resolves more details in precipitation. In addition, a too sparse network of precipitation/accumulation measurements could explain the low precipitation by Bales et al. (2009) or Ohmura and Reeh (1991) compared to Ettema et al. (2009). In any case, the mismatch of our simulated ice discharge over sector SE with that derived form Ettema et al. (2009) is probably due to differences in simulated precipitation fields between REMBO and RACMO2/GR over that sector.

Our range of valid model versions gives 326–479 $Gt yr^{-1}$ simulated total ice discharge. The lower estimate matches that by Reeh (1994), while the upper end of this range nearly equals the ice discharge derived from the surface mass balance data of Ettema et al. (2009). The relative small total ice discharge by Reeh (1994) corresponds to the rather small accumulation estimate of the Ohmura and Reeh (1991) compilation, which Reeh used together with the assumption that the GIS is in equilibrium to derive his discharge values. The data by Reeh (1994) can be regarded as roughly similar to pre-industrial, because it is based on accumulation, which contains several old data points, certainly before the 1990s. The Ohmura and Reeh (1991) (and the Bales et al., 2009) Greenland accumulation have smaller totals compared with the accumulation by Ettema et al. (2009), mainly due to higher accumulation in the sector SE. This might explain why our simulated total discharge for the GIS lies largely in between the two totals by Reeh (1994) and Ettema et al. (2009).

On the other end, the data from Ettema et al. (2009) represent average fields for the years 1958–2007, while the boundary conditions of REMBO are based on climatology

TCD
8, 1151–1189, 2014

from 1958 to 2001. Now from the beginning of 2000 a rather strong decline in GIS ice volume is observed from gravimetric satellite data (Velicogna, 2009). This change in volume of course violates our equilibrium assumption made for the RACMO2/GR data and we would have to add about 100 $Gt\,yr^{-1}$ to the ice discharge derived from the RACMO2/GR surface mass balance. This would make our upper estimate of total ice discharge somewhat too low compared to that by Ettema et al. (2009) if corrected for disequilibrium. Again, our estimate of the total ice discharge, if compared with findings by others, is not solely related to the quality of the ice discharge parameterization. It is also a problem of the right interpretation of the data and of the correct representation of precipitation in models.

6 Discussion

In spite of significant improvements of the simulated GIS topography with our discharge parameterization, for all of our simulations it was impossible to yield an error in ice thickness smaller than about 18 %. These rather large errors partly underline the limits of our ice discharge parameterization and modelling approach in general. We designed this parameterization as a workaround until a more comprehensive whole-Greenland glacial system approach becomes available. Of course, additional improvements are possible, like introducing a more physically based treatment of ice-marginal system including models for outlet glaciers and fjords. Nevertheless, note that the relative high error in ice thickness (up to 20 %) also results from the fact that this is a rather strong measure of the error in ice-sheet shape, compared to the error in ice area or in ice volume.

Although the model agrees reasonably well with observations overall, there are some significant biases in simulated ice discharge at the regional scale. For example, we have too much ice discharge in the northeastern and too little in the northwestern sector. The disagreements can be partly attributed to regional biases of simulated precipitation by REMBO and to difficulties in interpretation of the data used for comparison.

TCD
8, 1151–1189, 2014

When designing our constraints, we took the reduction in Eemian surface elevation upstream of the NEEM ice core from the NEEM community members (2013). In their statistics, the NEEM community members gave a one σ error for this value. In principle, one could have included the more uncertain values too by using the two σ range. Nonetheless, all of our simulations with valid parameter sets show a strong retreat of the ice in northern Greenland during Eemian times. Such a retreat strongly influences the local climate and might lead to an additional Eemian temperature rise over that region, although unlikely such vigorous as reported by the NEEM community members (2013). These and other uncertainties in Eemian temperature and precipitation will be examined in future work.

7 Conclusions

We introduced a new sub-grid scale ice discharge parameterization aimed at mimicking Greenland's fast outlet glaciers in a coarse resolution ice-sheet model. Our simulated ice discharge compares reasonably well with observations and other model estimates. The ice discharge parameterization enables us to simulate an ice sheet, whose shape is in good agreement with observations and whose partition between ice discharge and surface melt is in good agreement with state-of-the-art regional climate models.

We used various constraints to reduce the range of valid melt and discharge parameters of the REMBO-SICOPOLIS model: a shape constraint, a constraint on the mass balance partition between surface melt and ocean discharge (Robinson et al., 2011), and a palaeo-constraint on Greenland's surface elevation drop (upstream of the NEEM borehole) during the Eemian compared to present. We favoured a measure of ice thickness error at each grid point instead of just considering total Greenland area or volume, since it is a stronger measure of the ice-sheet shape.

The NEEM constraint showed to be an additional complementary constraint to the other two present-day constraints. It was the strongest constraint in controlling the upper end of the range of valid melt parameter values and thereby Greenland's

TCD
8, 1151–1189, 2014

contribution to Eemian sea-level rise. Taken individually, this constraint was also comparable to the shape constraint in determining the range of simulated present-day GIS margins. This demonstrates the important role of palaeo-climate information for determining the range of model parameters applicable for future prediction of the contribution of the GIS to sea level.

We can satisfy all constraints if our sub-grid scale ice discharge parameterization is included in a coarse resolution model in order to mimic small-scale fast processes. When using a shape-only constraints in a coarse resolution model without the parameterization of fast processes, we obtained a very unstable ice sheet – i.e., a temperature rise of as low as 0.25 °C was sufficient to melt the GIS almost completely on longer time scales. Applying the MBP constraint in a coarse resolution model without the sub-grid scale ice discharge parameterization, the model has about the same stability properties as with the discharge parameterization.

The inclusion of our ice discharge parameterization along with the above-described constraints leads to similar results concerning long-term stability as Robinson et al. (2012), with a decay threshold between 1.25 °C and 2.5 °C. Note that although this range is consistent with previous work (Robinson et al., 2012), it does not result from an exhaustive uncertainty analysis. An updated range comparable with Robinson et al. (2012) will be the provided in future work. Finally, complying with all three constraints leads to a GIS contribution to sea level rise during the Eemian compared to present-day in the range of 0.6–2.5 m, with an average of 1.4 m. Again, this range could widen if further uncertainties were included.

Acknowledgements. We would like to thank J. Ettema and M. van den Broeke for providing the RACMO2/GR surface mass balance data, as well as R. Bales and Q. Guo, who provided accumulation and precipitation data.

TCD
8, 1151–1189, 2014

References

Applegate, P. J., Kirchner, N., Stone, E. J., Keller, K., and Greve, R.: An assessment of key model parametric uncertainties in projections of Greenland Ice Sheet behavior, The Cryosphere, 6, 589–606, doi:10.5194/tc-6-589-2012, 2012. 1152

Bales, R. C., Guo, Q., Shen, D., McConnell, J. R., Du, G., Burkhart, J. F., Spikes, V. B., Hanna, E., and Cappelen, J.: Annual accumulation for Greenland updated using ice core data developed during 2000–2006 and analysis of daily coastal meteorological data, J. Geophys. Res., 114, D06116, doi:10.1029/2008JD011208, 2009. 1164, 1170

Bamber, J. L., Layberry, R. L., and Gogenini, S. P.: A new ice thickness and bed data set for the Greenland ice sheet, 1. Measurement, data reduction, and errors, J. Geophys. Res., 106, 33773–33780, 2001. 1155, 1169, 1188

Born, A. and Nisancioglu, K. H.: Melting of Northern Greenland during the last interglaciation, The Cryosphere, 6, 1239–1250, doi:10.5194/tc-6-1239-2012, 2012. 1154, 1155

Calov, R. and Ganopolski, A.: Multistability and hysteresis in the climate–cryosphere system under orbital forcing, Geophys. Res. Lett., 32, L21717, doi:10.1029/2005GL024518, 2005. 1167

Calov, R., Ganopolski, A., Claussen, M., Petoukhov, V., and Greve, R.: Transient simulation of the last glacial inception, Part I: glacial inception as a bifurcation of the climate system, Clim. Dynam., 24, 545–561, doi:10.1007/s00382-005-0007-6, 2005. 1162

Claussen, M., Mysak, L. A., Weaver, A. J., Crucifix, M., Fichefet, T., Loutre, M.-F., Weber, S. L., Alcamo, J., Alexeev, V. A., Berger, A., Calov, R., Ganopolski, A., Goosse, H., Lohman, G., Lunkeit, F., Mokhov, I. I., Petoukhov, V., Stone, P., and Wang, Z.: Earth system models of intermediate complexity: closing the gap in the spectrum of climate system models, Clim. Dynam., 18, 579–586, doi:10.1007/s00382-001-0200-1, 2002. 1169

Ettema, J., van den Broeke, M. R., van Meijgaard, E., van de Berg, W. J., Bamber, J. L., Box, J. E., and Bales, R. C.: Higher surface mass balance of the Greenland ice sheet revealed by high-resolution climate modeling, Geophys. Res. Lett., 36, L12501, doi:10.1029/2009GL038110, 2009. 1169, 1170, 1171, 1189

Ganopolski, A. and Calov, R.: The role of orbital forcing, carbon dioxide and regolith in 100 kyr glacial cycles, Clim. Past, 7, 1415–1425, doi:10.5194/cp-7-1415-2011, 2011. 1162

TCD
8, 1151–1189, 2014

Goelzer, H., Huybrechts, P., Loutre, M. F., Goosse, H., Fichefet, T., and Mouchet, A.: Impact of Greenland and Antarctic ice sheet interactions on climate sensitivity, Clim. Dynam., 37, 1005–1018, doi:10.1007/s00382-010-0885-0, 2011. 1152

Goelzer, H., Huybrechts, P., Fürst, J. J., Nick, F. M., Andersen, M. L., Edwards, T. L., Fettweis, X., Payne, A. J., and Shannon, S.: Sensitivity of Greenland ice sheet projections to model formulations, J. Glaciol., 59, 733–549, doi:10.3189/2013JoG12J182, 2013. 1153, 1154

Graversen, R. G., Drijfhout, S., Hazeleger, W., van de Wal, R., Bintanja, R., and Helsen, M.: Greenland's contribution to global sea-level rise by the end of the 21st century, Clim. Dynam., 37, 1427–1442, doi:10.1007/s00382-010-0918-8, 2011. 1152

Greve, R.: A continuum-mechanical formulation for shallow polythermal ice sheets, Philos. T. R. Soc. Lond. A, 355, 921–974, doi:10.1098/rsta.1997.0050, 1997. 1155

Greve, R.: On the response of the Greenland ice sheet to greenhouse climate change, Climatic Change, 46, 289–303, 2000. 1152

Greve, R., Saito, F., and Abe-Ouchi, A.: Initial results of the SeaRISE numerical experiments with the models SICOPOLIS and IcIES for the Greenland ice sheet, Ann. Glaciol., 52, 23–30, 2011. 1153

Hanna, E., Navarro, F. J., Pattyn, F., Domingues, C. M., Fettweis, X., Ivins, E. R., Nicholls, R. J., Ritz, C., Smith, B., Tulaczyk, S., Whitehouse, P. L., and Zwally, H. J.: Ice-sheet mass balance and climate change, Nature, 498, 51–59, doi:10.1038/nature12238, 2013. 1153

Helsen, M. M., van de Berg, W. J., van de Wal, R. S. W., van den Broeke, M. R., and Oerlemans, J.: Coupled regional climate–ice-sheet simulation shows limited Greenland ice loss during the Eemian, Clim. Past, 9, 1773–1788, doi:10.5194/cp-9-1773-2013, 2013. 1165

Huybrechts, P. and de Wolde, J.: The dynamic response of the Antarctic and Greenland ice sheets to multiple-century climatic warming, J. Climate, 12, 2169–2188, doi:10.1175/1520-0442(1999)012<2169:TDROTG>2.0.CO;2, 1999. 1152

Huybrechts, P., Letréguilly, A., and Reeh, N.: The Greenland ice sheet and greenhouse warming, Global Planet. Change, 3, 399–412, 1991. 1152

Joughin, I., Smith, B. E., Howat, I. M., Scambos, T., and Moon, T.: Greenland flow variability from ice-sheet-wide velocity mapping, J. Glaciol., 56, 415–430, 2010. 1158

Lipscomb, W. H., Fyke, J. G., Vizcaíno, M., Sacks, W. J., Wolfe, J., Vertenstein, M., Craig, A., Kluzek, E., and Lawrence, D. M.: Implementation and initial evaluation of the Glimmer Com-

TCD
8, 1151–1189, 2014

munity Ice Sheet Model in the Community Earth System Model, J. Climate, 26, 7352–7371, doi:10.1175/JCLI-D-12-00557.1, 2013. 1152, 1153
Moon, T. and Joughin, I.: Changes in ice front position on Greenland's outlet glaciers from 1992 to 2007, J. Geophys. Res., 113, F02022, doi:10.1029/2007JF000927, 2008. 1159
Moon, T., Joughin, I., Smith, B., and Howat, I.: 21st-century evolution of Greenland outlet glacier velocities, Science, 336, 576–578, doi:10.1126/science.1219985, 2012. 1159
NEEM community members: Eemian interglacial reconstructed from a Greenland folded ice core, Nature, 493, 489–494, doi:10.1038/nature11789, 2013. 1155, 1163, 1165, 1167, 1172
Nowicki, S., Bindschadler, R. A., Abe-Ouchi, A., Aschwanden, A., Bueler, E., Choi, H., Fastook, J., Granzow, G., Greve, R., Gutowski, G., Herzfeld, U., Jackson, C., Johnson, J., Khroulev, C., Larour, E., Levermann, A., Lipscomb, W. H., Martin, M. A., Morlighem, M., Parizek, B. R., Pollard, D., Price, S. F., Ren, D. D., Rignot, E., Saito, F., Sato, T., Seddik, H., Seroussi, H., Takahashi, K., Walker, R., and Wang, W. L.: Insights into spatial sensitivities of ice mass response to environmental change from the SeaRISE ice sheet modeling project II: Greenland, Geophys. Res. Lett., 118, 1025–1044, doi:10.1002/jgrf.20076, 2013. 1153
Ohmura, A. and Reeh, N.: New precipitation and accumulation maps for Greenland, J. Glaciol., 37, 140–148, 1991. 1170
Otto-Bliesner, B. L., Marshall, S. J., Overpeck, J. T., Miller, G. H., and Hu, A.: Simulating Arctic climate warmth and icefield retreat in the last interglaciation, Science, 311, 1751–1753, doi:10.1126/science.1120808, 2006. 1165
Petoukhov, V., Ganopolski, A., Brovkin, V., Claussen, M., Eliseev, A., Kubatzki, C., and Rahmstorf, S.: CLIMBER-2: a climate system model of intermediate complexity, Part I: model description and performance for present climate, Clim. Dynam., 16, 1–17, 2000. 1162
Price, S. F., Payne, A. J., Howat, I., and Smith, B. E.: Committed sea-level rise for the next century from Greenland ice sheet dynamics during the past decade, P. Natl. Acad. Sci. USA, 108, 8978–8983, doi:10.1073/pnas.1017313108, 2011. 1152
Quiquet, A., Ritz, C., Punge, H. J., and Salas y Mélia, D.: Greenland ice sheet contribution to sea level rise during the last interglacial period: a modelling study driven and constrained by ice core data, Clim. Past, 9, 353–366, doi:10.5194/cp-9-353-2013, 2013. 1165
Reeh, N.: Calving from Greenland glaciers: Observations, balance estimates of calving rates, calving laws, in: Report on the Workshop on the Calving Rate of West Greenland Glaciers in Response to Climate Change, edited by: Reeh, N., Danish Polar Center, Copenhagen, 85–102, 1994. 1157, 1169, 1170, 1189

TCD
8, 1151–1189, 2014

Ridley, J. K., Huybrechts, P., Gregory, J. M., and Lowe, J. A.: Elimination of the Greenland ice sheet in a high CO_2 climate, J. Climate, 18, 3409–3427, 2005. 1153

Rignot, E. and Mouginot, J.: Ice flow in Greenland for the International Polar Year 2008–2009, Geophys. Res. Lett., 39, L11501, doi:10.1029/2012GL051634, 2012. 1158

Rignot, E., Box, J. E., Burgess, E., and Hanna, E.: Mass balance of the Greenland ice sheet from 1958 to 2007, Geophys. Res. Lett., 35, L20502, doi:10.1029/2008GL035417, 2008. 1157, 1170, 1189

Robinson, A., Calov, R., and Ganopolski, A.: An efficient regional energy-moisture balance model for simulation of the Greenland Ice Sheet response to climate change, The Cryosphere, 4, 129–144, doi:10.5194/tc-4-129-2010, 2010. 1154, 1155, 1162, 1169

Robinson, A., Calov, R., and Ganopolski, A.: Greenland ice sheet model parameters constrained using simulations of the Eemian Interglacial, Clim. Past, 7, 381–396, doi:10.5194/cp-7-381-2011, 2011. 1153, 1154, 1156, 1161, 1162, 1163, 1166, 1167, 1168, 1172, 1187, 1188

Robinson, A., Calov, R., and Ganopolski, A.: Multistability and critical thresholds of the Greenland ice sheet, Nat. Clim. Change, 2, 429–432, doi:10.1038/NCLIMATE1449, 2012. 1153, 1154, 1167, 1168, 1173

Seddik, H., Greve, R., Zwinger, T., Gillet-Chaulet, F., and Gagliardini, O.: Simulations of the Greenland ice sheet 100 years into the future with the full Stokes model Elmer/Ice, J. Glaciol., 58, 427–440, doi:10.3189/2012JoG11J177, 2012. 1153

Shepherd, A., Ivins, E. R., Geruo, A., Barletta, V. R., Bentley, M. J., Bettadpur, S., Briggs, K. H., Bromwich, D. H., Forsberg, R., Galin, N., Horwath, M., Jacobs, S., Joughin, I., King, M. A., Lenaerts, J. T. M., Li, J. L., Ligtenberg, S. R. M., Luckman, A., Luthcke, S. B., McMillan, M., Meister, R., Milne, G., Mouginot, J., Muir, A., Nicolas, J. P., Paden, J., Payne, A. J., Pritchard, H., Rignot, E., Rott, H., Sorensen, L. S., Scambos, T. A., Scheuchl, B., Schrama, E. J. O., Smith, B., Sundal, A. V., van Angelen, J. H., van de Berg, W. J., van den Broeke, M. R., Vaughan, D. G., Velicogna, I., Wahr, J., Whitehouse, P. L., Wingham, D. J., Yi, D. H., Young, D., and Zwally, H. J.: A reconciled estimate of ice-sheet mass balance, Science, 338, 1183–1189, doi:10.1126/science.1228102, 2012. 1153

Stone, E. J., Lunt, D. J., Rutt, I. C., and Hanna, E.: Investigating the sensitivity of numerical model simulations of the modern state of the Greenland ice-sheet and its future response to climate change, The Cryosphere, 4, 397–417, doi:10.5194/tc-4-397-2010, 2010. 1153

TCD
8, 1151–1189, 2014

Stone, E. J., Lunt, D. J., Annan, J. D., and Hargreaves, J. C.: Quantification of the Greenland ice sheet contribution to Last Interglacial sea level rise, Clim. Past, 9, 621–639, doi:10.5194/cp-9-621-2013, 2013. 1152, 1154

Tarasov, L. and Peltier, W. R.: Greenland glacial history, borehole constraints, and Eemian extent, J. Geophys. Res., 108, 2143–2163, doi:10.1029/2001JB001731, 2003. 1154

Uppala, S. M., Kallberg, P. W., Simmons, A. J., Andrae, U., Bechtold, V. D., Fiorino, M., Gibson, J. K., Haseler, J., Hernandez, A., Kelly, G. A., Li, X., Onogi, K., Saarinen, S., Sokka, N., Allan, R. P., Andersson, E., Arpe, K., Balmaseda, M. A., Beljaars, A. C. M., van de Berg, L., Bidlot, J., Bormann, N., Caires, S., Chevallier, F., Dethof, A., Dragosavac, M., Fisher, M., Fuentes, M., Hagemann, S., Holm, E., Hoskins, B. J., Isaksen, L., Janssen, P. A. E. M., Jenne, R., McNally, A. P., Mahfouf, J. F., Morcrette, J. J., Rayner, N. A., Saunders, R. W., Simon, P., Sterl, A., Trenberth, K. E., Untch, A., Vasiljevic, D., Viterbo, P., and Woollen, J.: The ERA-40 re-analysis, Q. J. Roy. Meteor. Soc., 131, 2143–2163, doi:10.1256/qj.04.176, 2005. 1156

van de Wal, R. S. W. and Oerlemans, J.: Modelling the short-term response of the Greenland ice-sheet to global warming, Clim. Dynam., 13, 733–744, 1997. 1152

van den Berg, J., van de Wal, R. S. W., and Oerlemans, J.: A mass balance model for the Eurasian Ice Sheet for the last 120 000 years, Global Planet. Change, 61, 194–208, doi:10.1016/j.gloplacha.2007.08.015, 2008. 1156

Velicogna, I.: Increasing rates of ice mass loss from the Greenland and Antarctic ice sheets revealed by GRACE, Geophys. Res. Lett., 36, L19503, doi:10.1029/2009GL040222, 2009. 1171

Vizcaíno, M., Mikolajewicz, U., Jungclaus, J., and Schurgers, G.: Climate modification by future ice sheet changes and consequences for ice sheet mass balance, Clim. Dynam., 34, 301–324, doi:10.1007/s00382-009-0591-y, 2010. 1152

TCD
8, 1151–1189, 2014

Table 1. Temperature values of the threshold of decay of the Greenland ice sheet for a number of valid model parameters.

c_d	c_m [$W m^{-2}$]	Decay Threshold [°C]
0.8	−53	1.25
1.8	−60	1.75
1.2	−66	2.5

TCD
8, 1151–1189, 2014

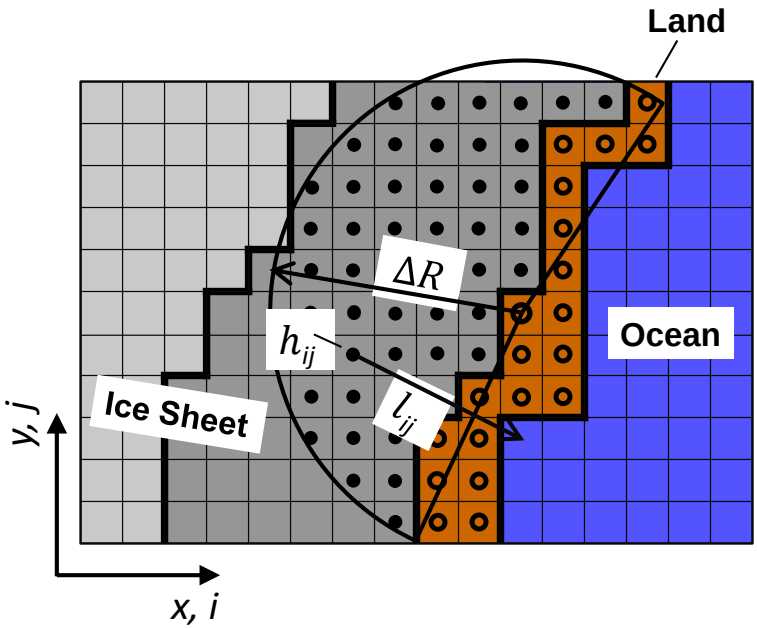

Fig. 1. Principle sketch of the discharge parameterization over a part of the horizontal computational domain. The gray shading shows the ice-covered cells, while the dark gray shaded area indicates the region over the ice sheet where the discharge parameterization applies. The (half) circle illustrates how that band with the width of about ΔR is determined in our scheme. Namely, the centre of such a circle is applied to every land point (open circles over the brown area). The smallest distance to the ocean l_{ij} is here depicted for one example ice grid point. It is determined for every grid point inside the band with width ΔR. For the discharge parameterization, the ice thickness h_{ij} and the smallest distance to the ocean l_{ij} are evaluated at grid points (i, j), see Eq. (2).

TCD
8, 1151–1189, 2014

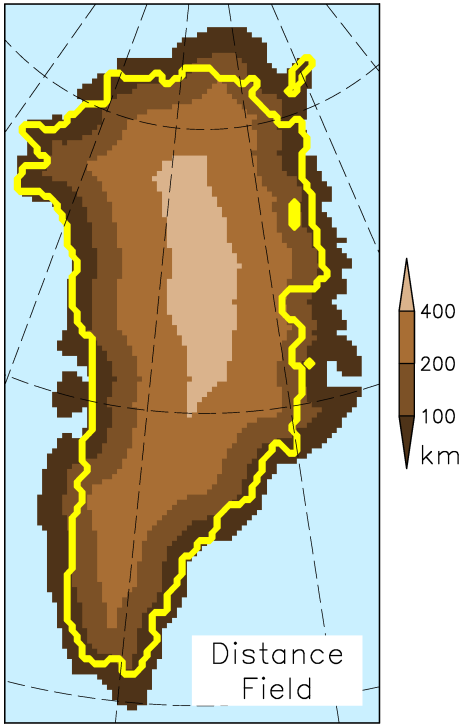

Fig. 2. Distance field over the entire Greenland area in km. It is determined by the minimal distance of every land grid point (ice free and ice covered ones) to the coast (first ocean grid point, see Fig. 1). It defines the length / in the discharge parameterization (Eq. 2). The yellow line indicates the ice margin of the present-day Greenland ice sheet.

TCD
8, 1151–1189, 2014

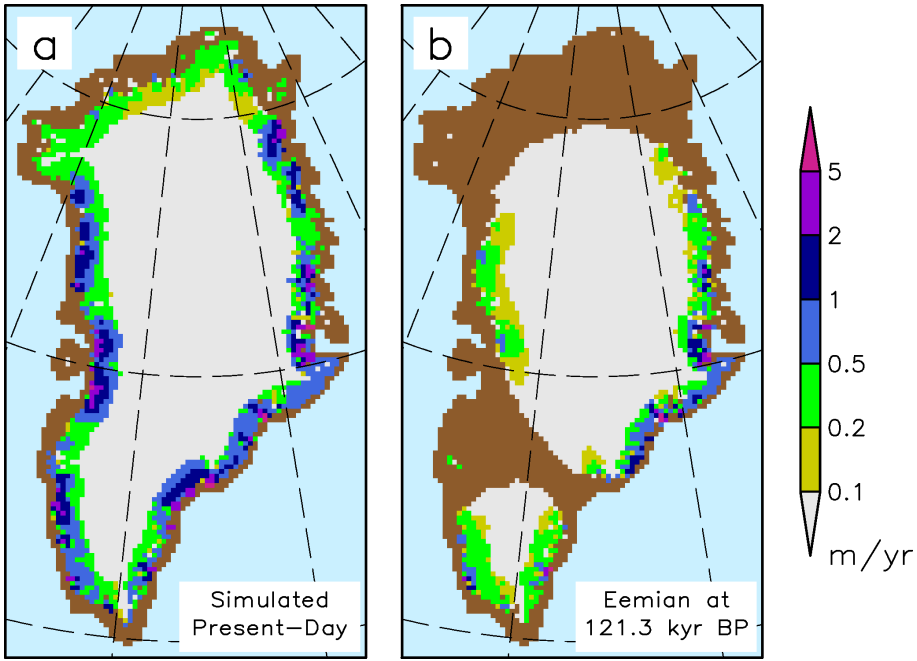

Fig. 3. Simulated ice discharge measured in $m yr^{-1}$ at **(a)** present-day and, **(b)** at Eemian from the model version with the most reduced Eemian ice sheet.

TCD
8, 1151–1189, 2014

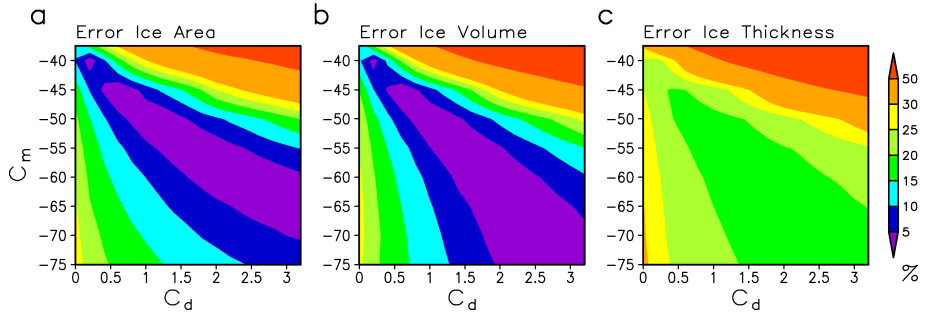

Fig. 4. Error measures for a modelled ice sheet in the $\{c_d\} \times \{c_m\}$ parameter space for $p = 1$ and $q = 3$ in Eq. (2). Relative errors in **(a)** ice area, **(b)** ice volume and **(c)** ice thickness, all in percent.

TCD
8, 1151–1189, 2014

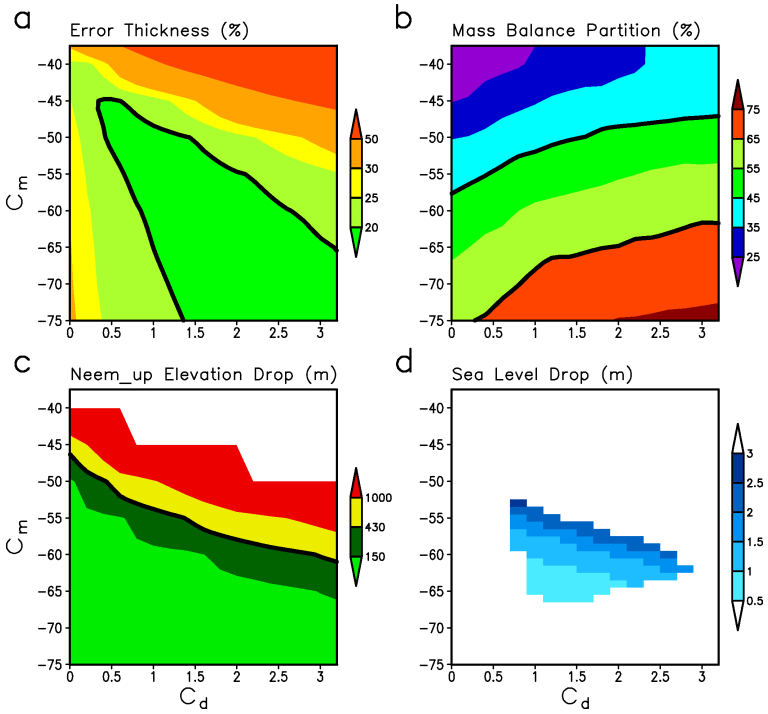

Fig. 5. Estimated constraints on the parameters c_d (ice discharge) and c_m (surface melt) illustrated with simulations for $p = 1$ and $q = 3$ together with our estimate of the GIS contribution to Eemian sea-level rise. **(a)** Relative error in ice thickness (%). **(b)** Mass balance partition (%). **(c)** Maximum elevation reduction during the Eemian compared to present-day 200 km upstream from NEEM (m). Here, regions where no Eemian ice is simulated at the upstream position of NEEM are displayed in white. **(d)** Simulated contribution of the Greenland ice sheet to sea-level rise between Eemian and present-day under our constraints. The black lines in panels **(a–c)** indicate our constraints: error values < 20 % for ice thickness, a 45 to 65 % range for mass balance partition and an Eemian to present-day surface elevation reduction of ≤ 430 m at the upstream position of NEEM.

TCD
8, 1151–1189, 2014

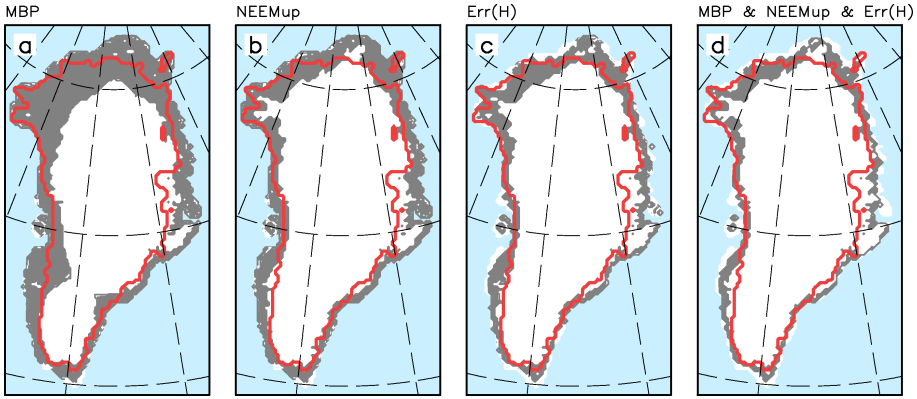

Fig. 6. Simulated geographical position of present-day ice margins for sets of runs with $p = 1$ and $q = 3$ in the discharge parameterization (gray areas) compared to observations (red line). **(a–c)** Single constraint applies: **(a)** mass balance partition, **(b)** elevation reduction during the Eemian referenced to present-day at the upstream position of NEEM, and **(c)** error in ice thickness. **(d)** All three constraints apply.

TCD
8, 1151–1189, 2014

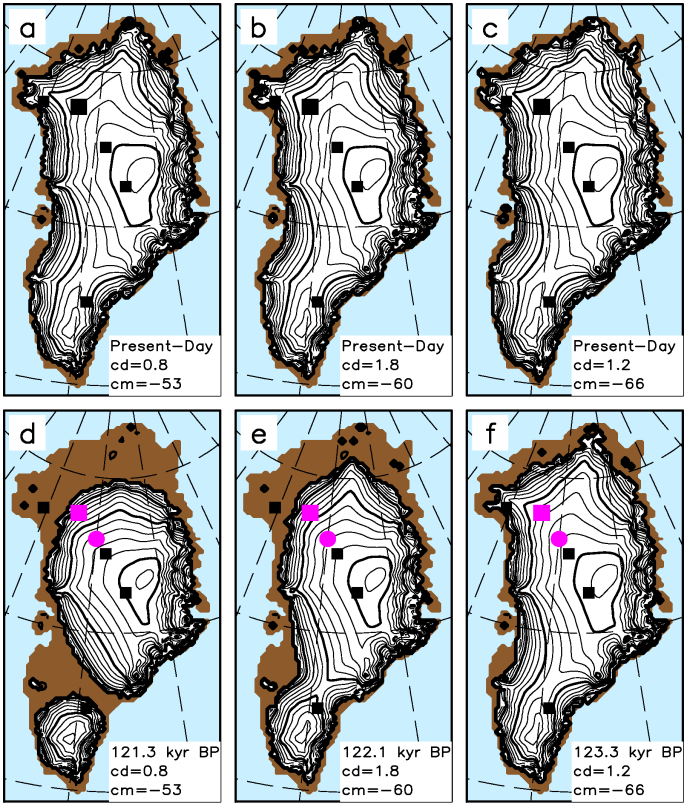

Fig. 7. Present-day **(a–c)** and Eemian **(d–f)** surface topography for varying melt and discharge parameters. Simulations correspond to those giving high medium and low contributions to Eemian sea-level rise (2.5 m, 1.5 m and 0.6 m), respectively. The Eemian snapshots correspond to times with the simulated minimum ice volume during the Eemian for the respective simulation. NEEM locations are marked in magenta (square for borehole and circle for upstream).

TCD
8, 1151–1189, 2014

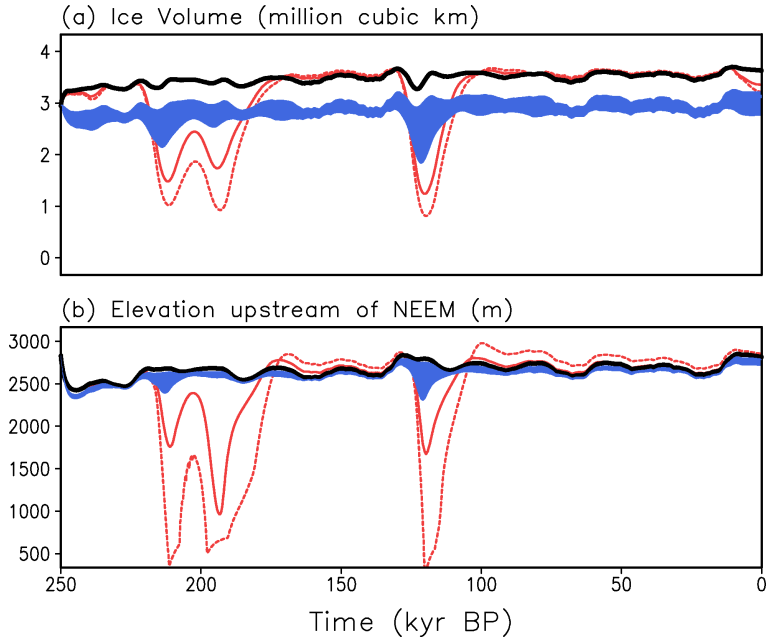

Fig. 8. Time series of the simulated Greenland ice sheet evolution during the last two glacial cycles. Blue shading represents the refined valid model versions including our discharge parameterization. Black and red lines show simulations without discharge parameterization ($c_d = 0$). Solid black lines indicate the central run of a set of optimized simulations by Robinson et al. (2011). The red lines are from simulations found via shape-only tuning of the melt parameter (see main text for explanation). In particular, a simulation with $c_m = -42\,\mathrm{W\,m^{-2}}$, found by minimizing err(H) (solid red line) and, alternatively, with $c_m = -40\,\mathrm{W\,m^{-2}}$, determined by minimizing err(V) (dashed red line). **(a)** Ice volume of the Greenland ice sheet. **(b)** Surface elevation at the NEEMup location.

TCD
8, 1151–1189, 2014

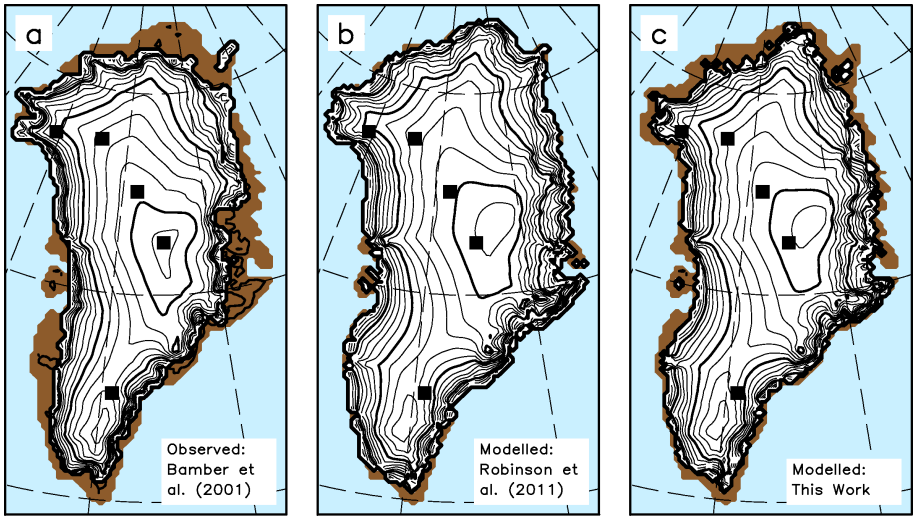

Fig. 9. Present-day Greenland ice sheet topography. **(a)** Observed data compilation by Bamber et al. (2001). **(b)** Simulation after Robinson et al. (2011). **(c)** Simulation from present work, given the parameter combination with smallest error in err(H), i.e. $c_d = 1.4$, $c_m = -60\,\mathrm{W\,m^{-2}}$.

TCD
8, 1151–1189, 2014

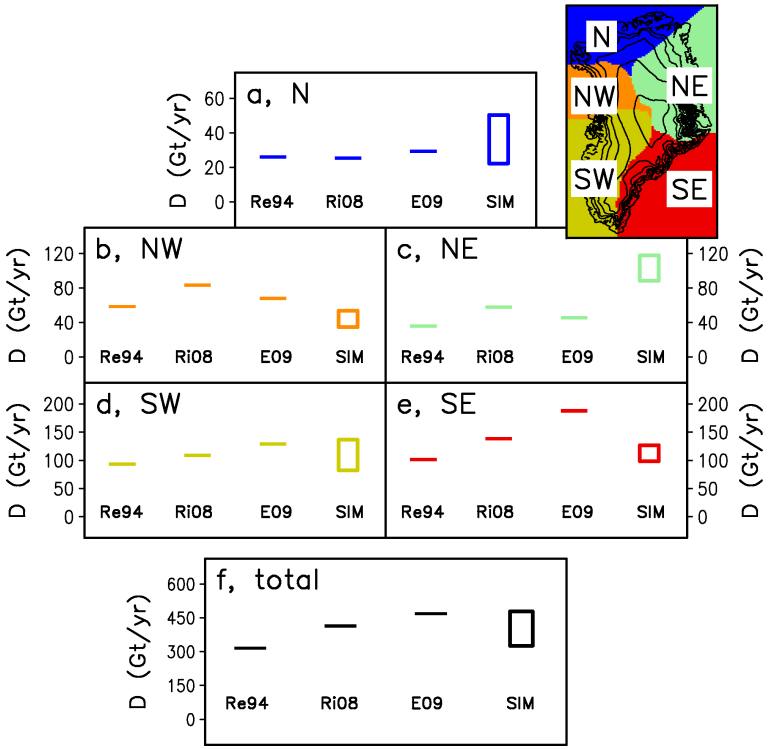

Fig. 10. Simulated ice discharge (open bars) vs. observations and findings by others (horizontal lines) at present-day (i.e., pre-industrial conditions). The heights of the open rectangles indicate the range of our simulated discharge. Acronyms are as follows: Re94: Reeh (1994), Ri08: Rignot et al. (2008) and E09: Ettema et al. (2009). SIM indicates our simulations. **(a–e)** Sectoral Greenland ice discharge in Gtyr^{-1} for the Northern (N), North-Western (NW), North-Eastern (NE), South-Western (SW), and South-Eastern (SE) parts (colours of the sectors are indicated in the inset). Note that the y-axes have different scales.

TCD
8, 1151–1189, 2014